nature materials

ARTICLES

https://doi.org/10.1038/s41563-020-00817-z

Check for updates

Defect reconfiguration in a Ti–Al alloy via electroplasticity

Shiteng Zhao[1,2,4], Ruopeng Zhang[1,2,4], Yan Chong[1,2], Xiaoqing Li[1,2], Anas Abu-Odeh[1], Eric Rothchild[1], Daryl C. Chrzan[1,3], Mark Asta[1,3], J. W. Morris Jr.[1] and Andrew M. Minor[1,2] ✉

It has been known for decades that the application of pulsed direct current can significantly enhance the formability of metals. However, the detailed mechanisms of this effect have been difficult to separate from simple Joule heating. Here, we study the electroplastic deformation of Ti–Al (7 at.% Al), an alloy that is uniquely suited for uncoupling this behaviour because, contrary to most metals, it has inherently lower ductility at higher temperature. We find that during mechanical deformation, electropulsing enhances cross-slip, producing a wavy dislocation morphology, and enhances twinning, which is similar to what occurs during cryogenic deformation. As a consequence, dislocations are prevented from localizing into planar slip bands that would lead to the early failure of the alloy under tension. Our results demonstrate that this macroscopic electroplastic behaviour originates from defect-level microstructural reconfiguration that cannot be rationalized by simple Joule heating.

Strong external stimuli may significantly alter the deformation behaviour of metals[1]. Research dating back to the 1960s has shown that many metals and alloys display dramatic increases in ductility when subjected to periodic electrical pulses during deformation[2–6]. Since the energy consumed by these pulses is often less than that required to heat the material to a temperature that offers comparable ductility[7,8], 'electroplastic' forming can be economically attractive and has been used to enhance the formability of titanium alloys[9], aluminium[10], magnesium alloys[11], zirconium alloys[12] and steels[13]. The imposition of a pulsed current may change the microstructure[12,14,15]. For example, imposing high-density current pulses may dissolve precipitates[16,17]. Research further suggests that electroplastic behaviour may reduce stress concentrations at twin boundaries[18]. More recently, an electrical pulsing treatment was successfully applied to modify the microstructure of additively manufactured parts[15].

While electroplasticity is well established experimentally, the underlying mechanisms are not yet clear. Several different possibilities have been explored, all based on the hypothesis that the electrical pulse momentarily lowers the flow stress. Initially it was believed that electroplasticity is nothing but thermal softening. However, further work showed that thermal effects could not fully explain the phenomenon[19,20], and it was proposed that the direct momentum transfer from the electron current to dislocations—that is, the 'electron wind force'—would facilitate dislocation slip[21,22]. Other researchers concluded that the electroplastic phenomenon is related closely to the thermal activation of dislocations[5,14], and suggested that electrical pulsing either lowers the energy barrier or increases the vibrational frequency of dislocations[19,21,22]. More recently, it was shown that the local energy states at the dislocation cores can be modified by the magnetic field induced by electrical pulses, which might lead to the de-pinning of dislocations from local obstacles[23,24]. However, evaluating these various athermal mechanisms is difficult since Joule heating occurs as soon as a current is applied and thermal softening intrudes. Historically, the threshold for electroplasticity has been loosely defined as the critical current density at which stress drops can be observed. However, this is complicated by the inertia effect of instrumented test systems where small load drops can be buried in the noise of bulk testing[14].

In the present work we studied electroplasticity in a Ti-Al alloy with 7 at.% Al (Ti-7Al). This material is particularly interesting in this context because of the influence of Al on the ductility of Ti. First, Al additions strengthen Ti and stabilize the α (hexagonal close-packed) phase[25]. However, there is a significant concomitant loss of ductility, which creates a need for process modifications to increase formability. This ductility loss is associated with a pronounced increase in the contribution of planar slip to the overall deformation. Planar slip is promoted by the short-range order of the Al (the preferred lattice occupation of specific elements over a length scale of several nearest neighbour distances) into coherent clusters with a $D0_{19}$ structure[26] and by the suppression of twinning in alloys with >5% Al due to an increase in the stacking fault energy[27]. As a result, the ductility of this alloy actually decreases on moderate heating (to 200–300 °C) as the pattern of slip becomes increasingly planar[28] and the extent of mechanical twinning diminishes[29].

Given that heating decreases ductility in this alloy, any significant electroplastic behaviour cannot be attributed to homogeneous Joule heating and must have other causes. To study the electroplastic effect, we performed tensile tests of Ti-7Al at ambient temperature under three conditions: (1) no current (room temperature, or RT), (2) a periodic pulse to a current of 0.5×10^3 A cm^{-2} with a square profile and a pulse duration of 100 ms (pulsing deformed) and (3) a continuous current of 0.5×10^3 A cm^{-2} (continuous current). The maximum current in the experiments was well below those used in previous studies of electroplasticity[1,4,7] and was chosen to minimize any Joule heating. The interval between two consecutive electrical pulses was 900 ms, which is sufficient for the sample to reach thermal equilibrium. The sample configuration and experimental details are given in the Methods. Typical stress–strain curves for the three tests are presented in Fig. 1a. An infrared camera was used to measure the temperature within the gauge length of the specimens (Fig. 1b–d). The steady current produced a temperature increase of

[1]Department of Materials Science and Engineering, University of California, Berkeley, CA, USA. [2]National Center for Electron Microscopy, Molecular Foundry, Lawrence Berkeley National Laboratory, Berkeley, CA, USA. [3]Materials Science Division, Lawrence Berkeley National Laboratory, Berkeley, CA, USA. [4]These authors contributed equally: Shiteng Zhao, Ruopeng Zhang. ✉e-mail: aminor@berkeley.edu

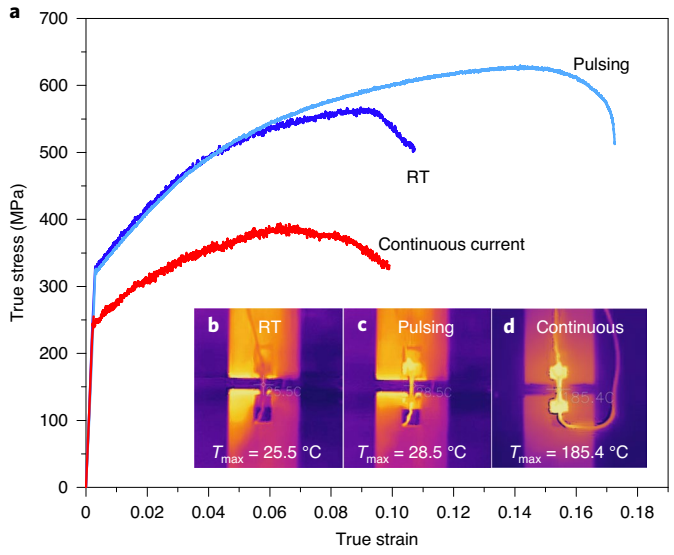

Fig. 1 | Mechanical and thermal measurements of the material at different conditions. a, Characteristic true stress versus true strain curves for Ti-7Al samples at room temperature, under continuous current and under electrical pulsing. **b**–**d**, Infrared images during testing showing the temperature distribution on the surface of the gauge section of the tensile specimen under each condition.

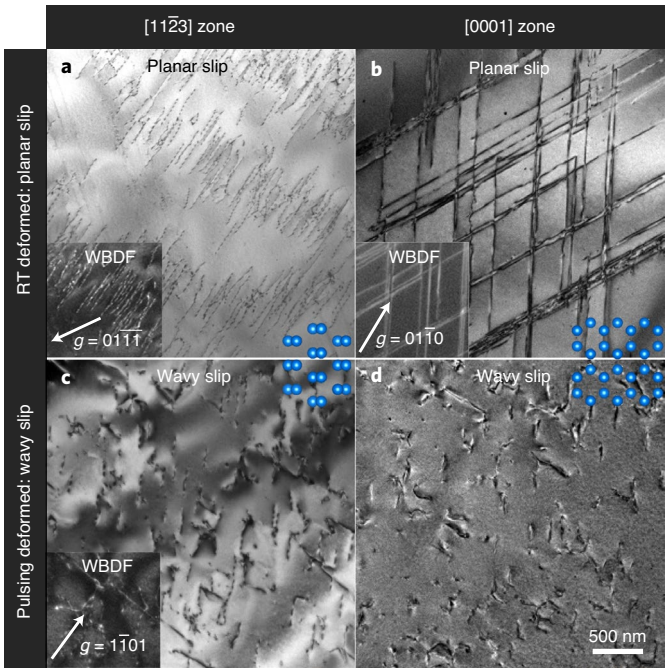

Fig. 2 | Comparison of dislocation morphology of samples pre-deformed to 5% of engineering strain. a, Bright-field TEM micrograph of tensile-deformed sample at room temperature shows planar slip configuration, with imaging condition close to [11$\bar{2}$3]zone axis. **b**, Dislocation network imaged from [0001] zone axis. **c**,**d**, Bright-field TEM micrographs of sample deformed with electrical pulsing, showing a relatively more homogeneous dislocation distribution. The imaging conditions in **c** and **d** are chosen to correspond to those of **a** and **b**, respectively. The two-beam, weak beam dark-field (WBDF) images of the dislocations are given in the insets of the corresponding bright-field images. In all the micrographs shown here, the tensile direction is perpendicular to the normal direction of the TEM samples and roughly pointing upwards. Schematic atomic structures are shown in blue for each orientation. The scale bar is the same for all the micrographs.

~200 °C, while the pulsed current caused only a very modest temperature rise ($\Delta T \approx 5$–10 °C). The data show that, despite the fact that the peak current in the periodic pulse was small compared to that used in prior work, the pulse produces a pronounced effect that improves both the tensile elongation and the maximum strength. This effect is specific to the pulsed current; a steady current of the same magnitude degrades both strength and ductility, presumably due to Joule heating.

Interestingly, the pulsed and RT specimens behave similarly until the strain reaches about ~5%, at which point the stress–strain curves diverge, with the strength of the RT specimen remaining well below that of the pulsed specimen for the remainder of the test. Consistent with its higher work-hardening rate, the pulsed specimen has a greater total elongation. To investigate the cause of this divergence we performed additional tensile tests that were interrupted at a strain of ~5% and examined the test specimens with high-resolution transmission electron microscopy (TEM). These observations revealed dramatic differences between the dislocation distributions in the RT and pulsed specimens. As shown in Fig. 2, the RT sample has the typical pattern produced by planar slip (Fig. 2a,b), while the pulsed sample contains a homogeneous, multidirectional dislocation network with a high population of jagged dislocation lines (Fig. 2c,d). This pattern is referred to as 'wavy slip' in other work. A **g**·**b** analysis shows that the dislocations are primarily of the ⟨**a**⟩ type on prismatic planes in both cases, but the dislocations in the pulsed specimen are heavily curved, indicating the occurrence of either local bow-out at discrete pinning points or cross-slip onto adjacent planes, while those in the RT specimen are aligned and relatively straight. The dislocation patterns are clearly differentiated by imaging near a [0001] zone axis: in the RT sample (Fig. 2b), the dislocations lie in planar bands on prismatic planes, creating a well-organized crystallographic network with 60° angles between the bands. The pulsed specimen shows no such planarity; the dislocations are curved and wavy, and the distribution is relatively homogeneous through the bulk. Apparently, the current does not alter the dislocation type in any obvious way, but rather changes the pattern of the dislocation network that develops during deformation.

To clarify this behaviour, we investigated whether this difference in the planarity of slip was present from the beginning of the deformation or resulted from some reconfiguration at about 5% strain. We conducted tensile tests that were interrupted at 2% strain and examined the dislocation distributions with TEM. The results are illustrated in Extended Data Fig. 1, which compares the dislocation patterns in the RT and pulsed samples at 2% strain, well before the stress–strain curves diverge. Slip in the RT specimen already appears planar, while that in the pulsed specimen is three-dimensional and wavy; the morphological difference between the two dislocation patterns seems to be established in the early stages of plastic deformation.

The next question for investigation is whether this beneficial dislocation pattern requires that the current be pulsed. The data for the sample tested under continuous current (Fig. 1) seems to show that it does. A continuous current with a density equal to that at the peak of the pulse not only does not improve the strength and elongation of the RT sample, but actually degrades them. Consistently, the steady current results in a highly planar dislocation pattern very similar to that in the RT specimen, as shown in Extended Data Fig. 2.

These results suggest that the beneficial electroplasticity exhibited by Ti-7Al is directly due to the suppression of planar slip by the current pulse. If this hypothesis is true, it follows that other ways of suppressing planar slip should have a similar effect. One possible

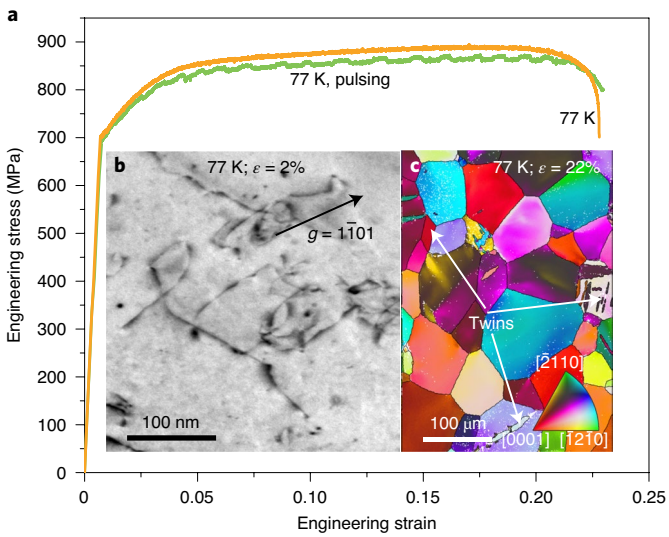

Fig. 3 | Cryogenic deformation shows similar behaviour as pulsing deformation at ambient temperature. a, Stress–strain curves of the Ti-7Al alloy at 77 K, showing a noticeable enhancement of strength and ductility, as compared with its room temperature behaviour in Fig. 1. Pulsing at 77 K does not lead to further improvement other than a periodic stress drop (note that we increase the pulse duration to 1 s to better illustrate the electrical pulses). **b**, TEM characterization of 2% (engineering strain, ε) pre-strained sample shows a wavy dislocation configuration, similar to the pulsing deformation at the ambient temperature (Fig. 1c,d). **c**, Electron backscattered diffraction (EBSD) inverse pole figure map of the sample after 22% of the pre-strain exhibits deformation twins. The similarity of the deformation mechanisms between 77 K and pulsing at ambient temperature indicates that the athermal component of electroplasticity is more important.

way of doing this is to lower the test temperature and increase the flow stress, reducing the tendency towards planar slip in these alloys[27]. We, therefore, conducted tensile tests in liquid nitrogen (77 K) with and without the current pulse. The results are presented in Fig. 3. The upper curve in Fig. 3a is the true stress–strain relation for the alloy tested at 77 K with no current. At this temperature the alloy exhibits high strength and ductility with a stress–strain behaviour very like that of the pulsed sample tested at ambient temperature. Moreover, TEM studies of the 77 K sample show a diffuse dislocation distribution similar to the pulsed specimen at ambient temperature (Fig. 3b). Figure 3a also includes the stress–strain curve of a sample pulsed at 77 K. While there does seem to be a slight softening of the alloy during the pulse, evidenced by the small periodic fluctuation in the stress–strain curve, the pulse does not increase ductility. In fact, there may be a slight decrease.

These results appear to establish that the beneficial electroplasticity exhibited by Ti-7Al when deformed in the presence of a periodic current pulse is directly due to the suppression of planar slip. As a consequence, the alloy retains a homogeneous distribution of active dislocations whose evolution produces sustainable work hardening and maintains uniform plastic deformation to high strain.

A final point that was investigated concerned the intrusion of mechanical twinning during the later stages of deformation. TEM analysis shows that prismatic slip by $\langle \mathbf{a} \rangle$-type dislocation dominates deformation to at least 5% true strain. However, it is not possible to construct five independent slips systems in a hexagonal close-packed crystal with $\langle \mathbf{a} \rangle$-type dislocations alone. Other mechanisms, such as mechanical twinning or slip by $\langle \mathbf{c}+\mathbf{a} \rangle$ dislocations, must be involved to accomplish significant plastic deformation in three dimensions. We, therefore, specifically investigated the contribution of twinning in the later stages of tensile strain, although the contrast of wavy versus planar dislocation configuration is still preserved, as shown in Extended Data Fig. 3.

At a strain of ~10%, the pulsed sample contains a recognizable density of twins whereas the RT deformed sample does not. Grain boundary misorientation analysis (Fig. 4a) indicates that the twins are primarily of $\{10\bar{1}2\}\langle\bar{1}011\rangle$ type with a misorientation of ~85° around the $\langle 1\bar{2}10\rangle$ axis. Figure 4b illustrates the nanoscale twins in the pulsed sample. The high-resolution TEM and scanning transmission electron microscopy (STEM) images (Fig. 4c–e) taken on the zone $[11\bar{2}0]$ indicates that these twins lie on $\{10\bar{1}2\}$ planes. The fraction of twin boundaries increases from 6% in the RT deformed sample to 11% in the pulsed sample (at room temperature) (Extended Data Figs. 4 and 5).

Since no significant twinning was detected in either the RT or pulsed sample at strains up to 5%, it is unlikely that twinning plays a vital role in the suppression of planar slip. However, twinning in the later stages of deformation does enhance ductility (the twinning-induced plasticity effect) and should contribute to the observed increase in tensile elongation. It also produces a more diffuse deformation, consistent with the observation that the pulsed sample exhibits necking prior to fracture (Extended Data Fig. 6a) while the RT deformed sample (Extended Data Fig. 6b) shows a pronounced shear fracture morphology.

While most previous interpretations of electroplasticity focus on mechanisms that enhance deformation by increasing the strain rate at a given stress (that is, by softening the material), in the present case the current pulse has the opposite effect. It hardens the material. Specifically, it increases the rate of work hardening so that plastic instability and necking are forestalled to increase strength and ductility.

Moreover, it is reasonably clear what the current pulse does to achieve this effect. It 'hardens' the material by frustrating the development of planar slip that softens it. The pulsed current maintains a diffuse, three-dimensional dislocation pattern of the sort that also produces high strength and ductility in the sample tested at 77 K in the absence of current. However, it is not yet clear how it does this. Pending further research, we can provide only a general discussion of the mechanisms that may be involved. Note that an appropriate explanation must explain not only how a current disrupts planar slip, but why a relatively modest pulsed current does this while a steady current of the same magnitude does not.

The likely cause of the pronounced planar slip in Ti-7Al seems clear from prior research[30–32]. The Al atoms in this alloy undergo short-range order and tend to cluster into coherent domains with a $D0_{19}$ structure. Lattice dislocations that cut through these domains create planar defects (diffuse anti-phase boundaries, or DAPB). If a second lattice dislocation passes through on the same glide plane, it partially restores the diffuse $D0_{19}$ and, therefore, moves easily through the ordered domain, so dislocations tend to cut the domain in pairs at a lowered value of the critical shear stress. Sequential dislocation cutting leads to the gradual destruction of order on the active glide plane, so following dislocations glide on the same plane at still lower critical stress[33]. These mechanisms promote planar slip. This theory is corroborated by evidence such as the observation of dislocation pairs as expected from the creation and destruction of diffuse anti-phase boundaries and by characterization of the short range ordered (SRO) structures with neutron diffraction[29] and energy-filtered transmission electron microscopy[26].

Planar slip in Ti-Al alloys is also facilitated by heating to moderate temperature since the greater dislocation mobility at higher temperature makes it easier for groups of dislocations to organize and maintain planar arrays. The higher flow stress and lower dislocation mobility when Ti-Al alloys are deformed at lower temperature favours slip activation on multiple planes, cross-slip, activation of alternative dislocation types ($\langle \mathbf{c}+\mathbf{a} \rangle$ dislocations) and significant

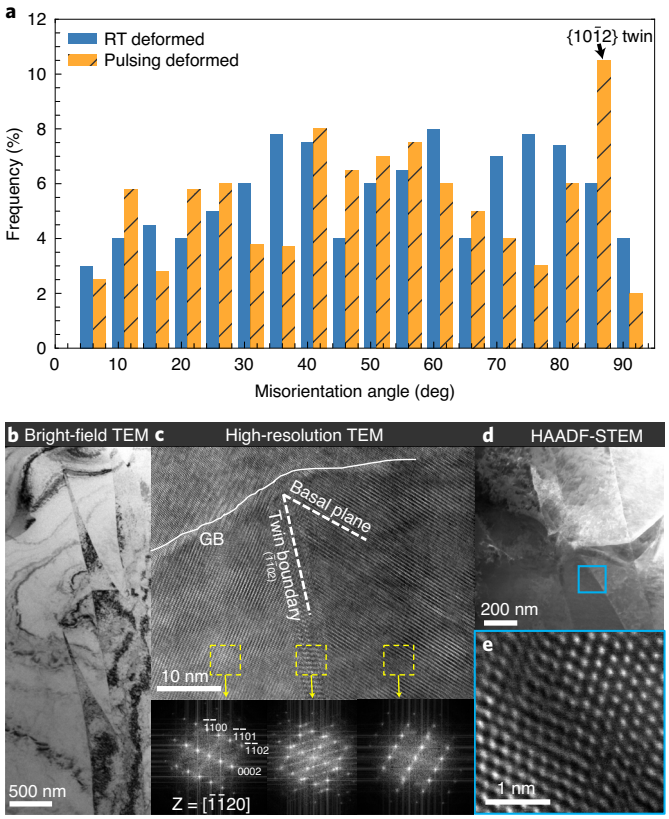

Fig. 4 | Characterization of the deformation twinning in the electrical-biasing deformed sample. a, EBSD misorientation angle analysis of the grain boundaries at an engineering strain of around 10%. The {10$\bar{1}$2} twin is marked by the 85° misorientation angle. **b**, Bright-field TEM image of the deformation twins. **c**, High-resolution TEM image on the [11$\bar{2}$0] zone in the vicinity of the twin boundary. Insets, crystallographic analysis indicates that these twins are of {10$\bar{1}$2} type with an ~85° misorientation. **d**, High-angle annular dark field, STEM (HAADF-STEM) image in the same region. **e**, The high-resolution STEM image of the twinned area (boxed in **d**) showing the atomic picture of the {10$\bar{1}$2} twin.

twinning, all of which promote a three-dimensional deformation pattern with a large, sustained work-hardening coefficient.

If we consider the various possible mechanisms of electroplasticity that have been proposed in prior work to explain the phenomenon in other materials[1–3,15], it is helpful to consider the usual Arrhenius equation for thermally activated dislocation plasticity:

$$\dot{\gamma} = \dot{\gamma}_0 \exp\left[-\frac{\Delta H(\tau)}{kT}\right] \quad (1)$$

where $\dot{\gamma}$ is the shear strain rate, $\Delta H(\tau)$ is the activation energy (a decreasing function of the applied stress, τ) and $\dot{\gamma}_0$ is a pre-exponential factor that includes the attempt frequency and the incremental strain per activation event. k is the Boltzmann constant and T is the temperature. It has been suggested that (1) Joule heating by the electrical current will soften the materials by increasing T, (2) direct dislocation–current interactions (the 'electron wind') will lower $\Delta H(\tau)$ by increasing the effective stress, τ, and may also increase the pre-exponential factor by increasing the slip distance per activation event and (3) rate effects associated with the periodic pulse may increase the effective attempt frequency.

There are two generic mechanisms that operate on the dislocation network to promote cross-slip in preference to planar slip: altering the stress state to promote cross-slip or changing the structure of the dislocation core so that it moves more easily on alternate planes. The stress can be significantly affected by thermal gradients and may also be affected by the current itself. The most obvious source of thermal gradients is inhomogeneous Joule heating due to some combination of inhomogeneity in the distribution of current and heterogeneities in the local value of the resistivity. Persistent thermal gradients seem unlikely under either a steady current or during a pulse (see Supplementary Information for estimates), so that if thermal gradients are inducing cross-slip, they must be only transient gradients that arise during the build-up or draw-down of the current at the beginning or end of the pulse.

Another potential source of a stress that promotes cross-slip is the momentum transfer from the current itself, the electron wind. However, the magnitude of this stress is very small in the case studied here. The stress is[7],

$$\tau_{ew} \approx \frac{m_e v_F j}{3e} \quad (2)$$

where m_e, v_F, j and e are the electron mass, Fermi velocity, current density and electron charge, respectively. Given a current density of 0.5×10^3 A cm^{-2}, the stress due to the electron wind stress is only 2.8 Pa, too small to have a significant influence on the dislocation even if directed perpendicular to the slip plane. Moreover, the effect of the electron wind (or a similar effect of enhanced cross-slip due to electromigration-induced climb) should appear in the steady test as well as the pulsed tests and should be more pronounced under steady current since the integrated flux of vacancies is larger with a steady current. In a similar manner, an estimate of the magnetostriction effect suggests a negligible contribution (Supplementary Information).

Still another possible origin of the observed dislocation reconfiguration is that the current pulse promotes twinning, which changes the local stress state and promotes cross-slip. While it is true that there is evidently more twinning in the pulsed sample than in the RT sample, this twinning appears fairly late in the test. No twinning was observed in the samples tested to 2% strain even though the difference in the dislocation pattern was well established by that point in the test. The evidence suggests that the more extensive twinning in the pulsed sample is a consequence of the dislocation pattern rather than its cause; the pulsed sample hardens to a higher flow stress that drives twinning as a preferred deformation mode.

Twinning is a stress-induced process and inherently athermal[34]. Avoiding stress concentration on unfavourable planes eventually leads to the nucleation of twins once a critical stress is reached. Electrical pulsing promotes a homogeneous deformation by enhancing cross-slip or dissolving the SRO domains, which favours the activation of twins since it allows for the stress to build up for mechanical twinning. However, planar slip in the RT deformed and continuous current deformed samples is unfavourable, since the stress localization in the prismatic plane does not correlate to any twin systems in hexagonal metals. At 77 K, the stress level is much higher, and thus it is easier for the alloy to undergo twinning[35]. A comparison of the twinning ability under different loading conditions is shown in Extended Data Fig. 4; both pulsing and cryogenic deformation promote twining, whereas continuous current and room temperature deformation supress twins.

Lastly, a generic way in which the current can change the dislocation pattern is through its effect on the microstructure. If the planar slip is due to domains of short-range order, then the modification or dissolution of these domains could dramatically change the tendency towards planar slip. However, for these SRO-related mechanisms (see Supplementary Information for details) to be the cause of the electroplasticity observed here, they must not only be sufficiently potent to disrupt planar slip but also explain why pulsing is effective while a steady current is not. A possible explanation

may lie in the thermal consequence of the current; in contrast to the steady current, pulsing imposes the current without significantly heating the specimen. Since moderate heating is known to promote planar slip in this alloy, Joule heating by the steady current may eliminate the beneficial effect of the current.

Finally, while the change in the dislocation pattern is the evident cause of the pronounced, beneficial electroplasticity in the alloy studied here, it does not follow that this mechanism is the universal cause of electroplasticity. Other plausible mechanisms have been proposed and may well be valid for other alloys or in other situations. However, it does follow that investigations of electroplasticity should pay close attention to the effect of the current or current pulse on the evolution of the dislocation pattern since it may play an important role.

In conclusion, we investigated the electroplastic behaviour of a Ti-7Al alloy, which is uniquely suited to differentiate simple Joule heating from electrical pulsing with regards to defect configuration. We have shown that the defect configuration can be dramatically modified by the application of pulsed currents, from localized planar slip to homogeneous wavy slip. A schematic illustration of the dislocation reconfiguration is presented in Extended Data Fig. 7. Such a sharp transition in microstructure leads to beneficial effects in terms of enhancing the ductility of the material. A variety of plausible mechanisms are qualitatively evaluated. Our investigation demonstrates that the macroscopic electroplastic behaviour originates from defect-level microstructure reconfiguration, which cannot be rationalized by simple Joule heating. It also suggests that the critical threshold for electroplasticity may be much lower than the critical current that marked the drop in flow stress. Since this mechanism enhances strength and ductility by changing the dislocation pattern during deformation, it is expected to apply only to materials whose ductility is limited by the deformation pattern, the most obvious being materials that deform by planar or otherwise markedly heterogeneous slip. The candidate materials we are likely to test in the near future include other alloys with pronounced short-range order; face-centred cubic alloys with naturally planar slip, including austenitic steels and high entropy alloys; and alloys that are age-hardened with coherent precipitates, including aluminium alloys and Fe- and Ni-based superalloys. Our discoveries not only provide new insights on the physical origins of the electroplasticity, but also may help refine electrical pulsing treatment for relevant alloys as a more affordable processing route for industrial applications.

Online content

Any methods, additional references, Nature Research reporting summaries, source data, extended data, supplementary information, acknowledgements, peer review information; details of author contributions and competing interests; and statements of data and code availability are available at https://doi.org/10.1038/s41563-020-00817-z.

Received: 21 April 2020; Accepted: 1 September 2020;
Published online: 05 October 2020

References

1. Conrad, H. Electroplasticity in metals and ceramics. *Mater. Sci. Eng. A* **287**, 276–287 (2000).
2. Troitskii, O. A. Electromechanical effect in metals. *JETP Lett.* **10**, 11 (1969).
3. Troitskii, O. A. Effect of the electron state of a metal on its mechanical properties and the phenomenon of electroplasticity. *Strength Mater.* **9**, 35–45 (1977).
4. Okazaki, K., Kagawa, M. & Conrad, H. An evaluation of the contributions of skin, pinch and heating effects to the electroplastic effect in titatnium. *Mater. Sci. Eng.* **45**, 109–116 (1980).
5. Conrad, H., Sprecher, A. F., Cao, W. D. & Lu, X. P. Electroplasticity—the effect of electricity on the mechanical properties of metals. *JOM* **42**, 28–33 (1990).
6. Andre, D. et al. Investigation of the electroplastic effect using nanoindentation. *Mater. Des.* **183**, 108153 (2019).
7. Xiang, S. & Zhang, X. Dislocation structure evolution under electroplastic effect. *Mater. Sci. Eng. A* **761**, 138026 (2019).
8. Waryoba, D., Islam, Z., Wang, B. & Haque, A. Low temperature annealing of metals with electrical wind force effects. *J. Mater. Sci. Technol.* **35**, 465–472 (2019).
9. Sheng, Y. et al. Application of high-density electropulsing to improve the performance of metallic materials: mechanisms, microstructure and properties. *Materials* **11**, 185 (2018).
10. Li, W. et al. Non-octahedral-like dislocation glides in aluminum induced by athermal effect of electric pulse. *J. Mater. Res.* **31**, 1193–1200 (2016).
11. Wang, X. et al. Current-induced ductility enhancement of a magnesium alloy AZ31 in uniaxial micro-tension below 373 K. *Materials* **12**, 111 (2019).
12. Islam, Z., Wang, B. & Haque, A. Current density effects on the microstructure of zirconium thin films. *Scr. Mater.* **144**, 18–21 (2018).
13. Zhao, Y. et al. Electropulsing strengthened 2GPa boron steel with good ductility. *Mater. Des.* **43**, 195–199 (2013).
14. Sprecher, A. F., Mannan, S. L. & Conrad, H. Overview no. 49. *Acta Metall.* **34**, 1145–1162 (1986).
15. Noell, P. J., Rodelas, J. M., Ghanbari, Z. N. & Laursen, C. M. Microstructural modification of additively manufactured metals by electropulsing. *Addit. Manuf.* **33**, 101128 (2020).
16. Qin, R. S. & Bhowmik, A. Computational thermodynamics in electric current metallurgy. *Mater. Sci. Technol.* **31**, 1560–1563 (2015).
17. Jiang, Y., Tang, G., Shek, C., Zhu, Y. & Xu, Z. On the thermodynamics and kinetics of electropulsing induced dissolution of β-Mg17Al12 phase in an aged Mg-9Al-1Zn. *Acta Mater.* **57**, 4797–4808 (2009).
18. Savenko, V. V. Electroplastic deformation by twinning metals. *Acta Mech. Autom.* **12**, 259–264 (2018).
19. Kravchenko, V. Y. Effect of directed electron beam on moving dislocations. *Sov. Phys. JETP* **24**, 1135–1142 (1967).
20. Roshchupkin, A. M. & Bataronov, I. V. Physical basis of the electroplastic deformation of metals. *Russ. Phys. J.* **39**, 230–236 (1996).
21. Klimov, K., Shnyrev, G. & Novikov, I. Electroplasticity in metals. *J. Sov. Phys. Dokl.* **19**, 787–788 (1975).
22. Roshchupkin, A. M., Miloshenko, V. E. & Kalinin, V. E. The electron retardation of dislocations in metals. *Fiz. Tverd. Tela* **21**, 909–910 (1979).
23. Molotskii, M. & Fleurov, V. Work hardening of crystals in a magnetic field. *Philos. Mag. Lett.* **73**, 11–15 (1996).
24. Molotskii, M. I. Theoretical basis for electro- and magnetoplasticity. *Mater. Sci. Eng. A* **287**, 248–258 (2000).
25. Lütjering, G. G. & Williams, J. C. *Titanium* (Springer, 2010).
26. Zhang, R. et al. Direct imaging of short-range order and its impact on deformation in Ti-6Al. *Sci. Adv.* **5**, eaax2799 (2019).
27. Williams, J. C., Baggerly, R. G. & Paton, N. E. Deformation behavior of HCP Ti-Al alloy single crystals. *Metall. Mater. Trans. A* **33**, 837–850 (2002).
28. Venkataraman, A. et al. Study of structure and deformation pathways in Ti-7Al using atomistic simulations, experiments, and characterization. *Metall. Mater. Trans. A* **48**, 2222–2236 (2017).
29. Fitzner, A. et al. The effect of aluminium on twinning in binary alpha-titanium. *Acta Mater.* **103**, 341–351 (2016).
30. Conrad, H. On the strengthening of titanium by aluminum. *Scr. Metall.* **7**, 509–512 (1973).
31. Neeraj, T., Holc, D. H., Daehn, G. S. & Mills, M. J. Phenomenological and microstructural analysis of room temperature creep in titanium alloys. *Acta Mater.* **48**, 1225–1238 (2000).
32. Neeraj, T. & Mills, M. J. Observation and analysis of weak-fringing faults in Ti-6 wt% Al. *Philos. Mag. A* **82**, 779–802 (2002).
33. van de Walle, A. & Asta, M. First-principles investigation of perfect and diffuse antiphase boundaries in HCP-based Ti-Al alloys. *Metall. Mater. Trans. A* **33**, 735–741 (2002).
34. Lubarda, V. A., Meyers, M. A. & Vo, O. The onset of twinning in metals: a constitutive description. *Acta Mater.* **49**, 4025–4039 (2001).
35. Moskalenko, V. A., Startsev, V. I. & Kovaleva, V. N. Low temperature peculiarities of plastic deformation in titanium and its alloys. *Cryogenics* **20**, 503–508 (1980).

Methods

Materials. TIMET provided the material used in this study. The raw material was argon, arc double melted and then forged to a square at 1,125 °C before water quenching. The square was then rolled at 910 °C. The nominal composition of the ingot material was Ti with 7 at.% Al. The buttons were heat treated at 840 °C for 2 h (~45 °C below the β-transus) to give an equiaxed microstructure with an average grain size of 80 μm. No preferred crystallographic orientations were observed.

Tensile testing. The tensile tests were performed using an MTS multifunctional mechanical tester (Model 43). The miniature dogbone-shaped tensile specimen with a gauge dimension of 1.8 mm × 0.8 mm × 5.1 mm was prepared with electrical discharge machining. A nominal strain rate of $10^{-3}\,s^{-1}$ was used for all the experiments. It has been proven that the results from these miniature samples are similar to those with a standardized sample. The detailed CAD plot of our sample geometry is shown in Extended Data Fig. 8. The dogbone-shaped tensile specimen was cut by an electro-discharge-machining method and the damage layer was mechanically polished away before mechanical testing. The region that is subjected to TEM observation is located in the centre of the sample and thus the mechanical damage introduced by electro-discharge machining is neglectable in our observation.

Thermal imaging. A Keysight B2961A 6.5 digit low noise power supply was used to provide the direct current with desired pulse shape ($0.5 \times 10^3\,A\,cm^{-2}$ peak current density, square pulse with a pulse duration of 100 ms). The sample fixture is insulated from the loading cell. A FLIR One Pro infrared camera was used to record the temperature distribution along the gauge length of the tensile sample during the mechanical testing. A video showing the specimen subjected to pulsed and continuous currents is provided in Supplementary Video 1.

EBSD measurement. The twinning frequency of materials subjected to different loading conditions was studied by EBSD. A FEI Strata 235 scanning electron microscope equipped with an EDAX EBSD detector operated at 20 kV was used for EBSD scans with a step size of 500 nm, and a field of view of 200 μm × 500 μm (within the gauge region in the tensile sample). The sample surfaces were electrochemically polished using a solution of 6% perchloric acid and 94% methanol. Orientation maps and twin boundary frequency plots were generated using the commercial EDAX EBSD analysis software.

TEM and STEM characterization. The deformation microstructure of the material was subjected to TEM observations to identify the twinning and dislocation behaviours. A 300 kV FEI TitanX TEM instrument was used to conduct the bright-field imaging and high-resolution TEM observations of twin boundaries and dislocations. The high-resolution STEM images were taken in the TEAM I microscope, which is both probe and image aberration corrected. The samples for TEM observations were polished with a Fischione Twin Jet Electropolisher (Model 110) to electron transparency using a solution of 6% perchloric acid and 94% methanol at −40 °C at approximately 30 V.

Data availability

The data that support the findings of this study are available from the corresponding author upon reasonable request.

Acknowledgements

We gratefully acknowledge funding from the US Office of Naval Research under grant no. N00014-17-1-2283. Work at the Molecular Foundry was supported by the Office of Science, Office of Basic Energy Sciences, of the US Department of Energy under contract no. DE-AC02-05CH11231.

Author contributions

S.Z. and A.M.M. proposed the experiments. S.Z., R.Z. and Y.C. performed the mechanical testing with electrical pulsing. S.Z. and R.Z. conducted the TEM and high-resolution STEM characterization of the resultant dislocation structures and twins. S.Z. conducted the EBSD. E.R. and D.C.C. estimated the magnetostriction and thermal diffusivity effects. R.Z., A.A. and X.L. assisted with the literature review. A.A. and M.A. provided the electrical free energy discussion. S.Z., J.W.M. and A.M.M. drafted the manuscript and all the authors contributed to the discussions. J.W.M. and A.M.M. supervised the project.

Competing interests

The authors declare no competing interests.

Additional information

Extended data is available for this paper at https://doi.org/10.1038/s41563-020-00817-z.

Supplementary information is available for this paper at https://doi.org/10.1038/s41563-020-00817-z.

Correspondence and requests for materials should be addressed to A.M.M.

Reprints and permissions information is available at www.nature.com/reprints.

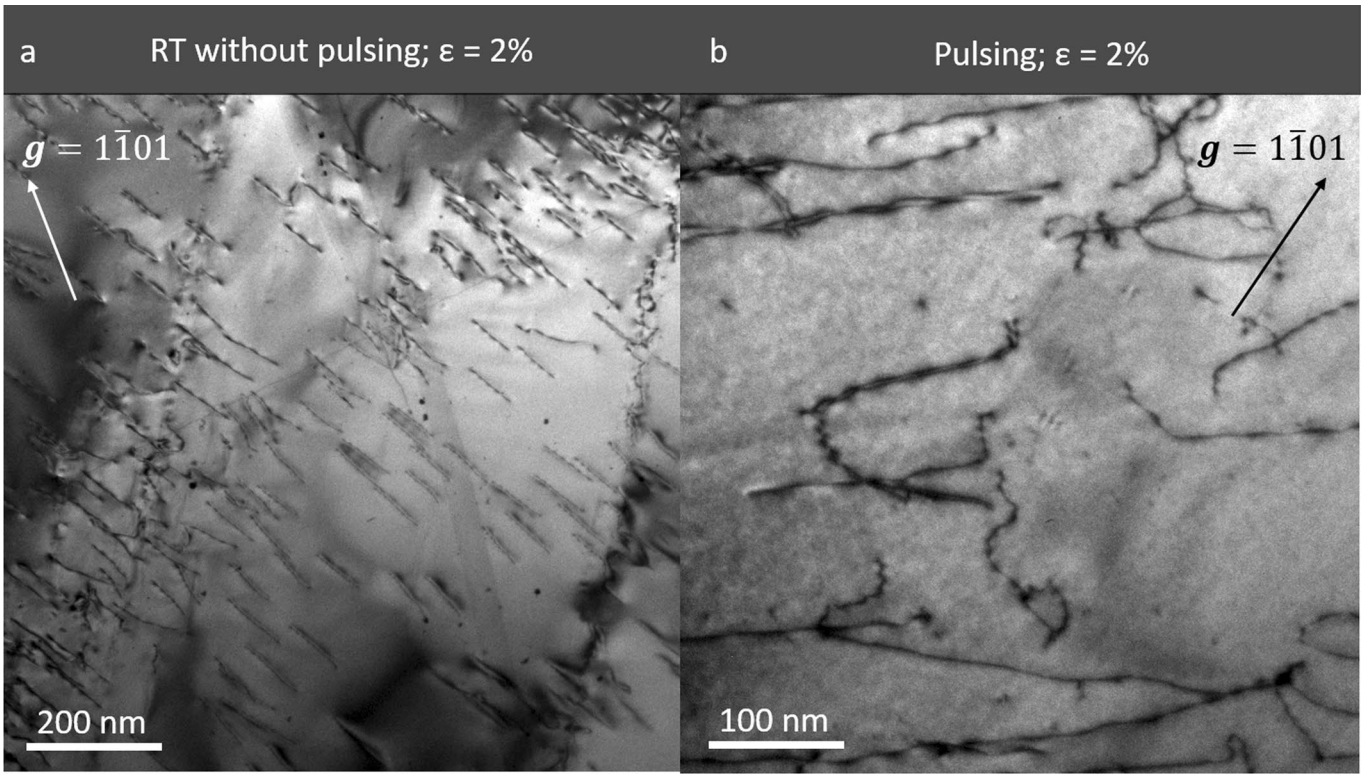

Extended Data Fig. 1 | Dislocation morphology of Ti-7Al subjected to 2% of plastic strain using different loading conditions. a, room temperature without pulsing shows planar dislocation configuration; (**b**) pulsing deformed showing wavy slip.

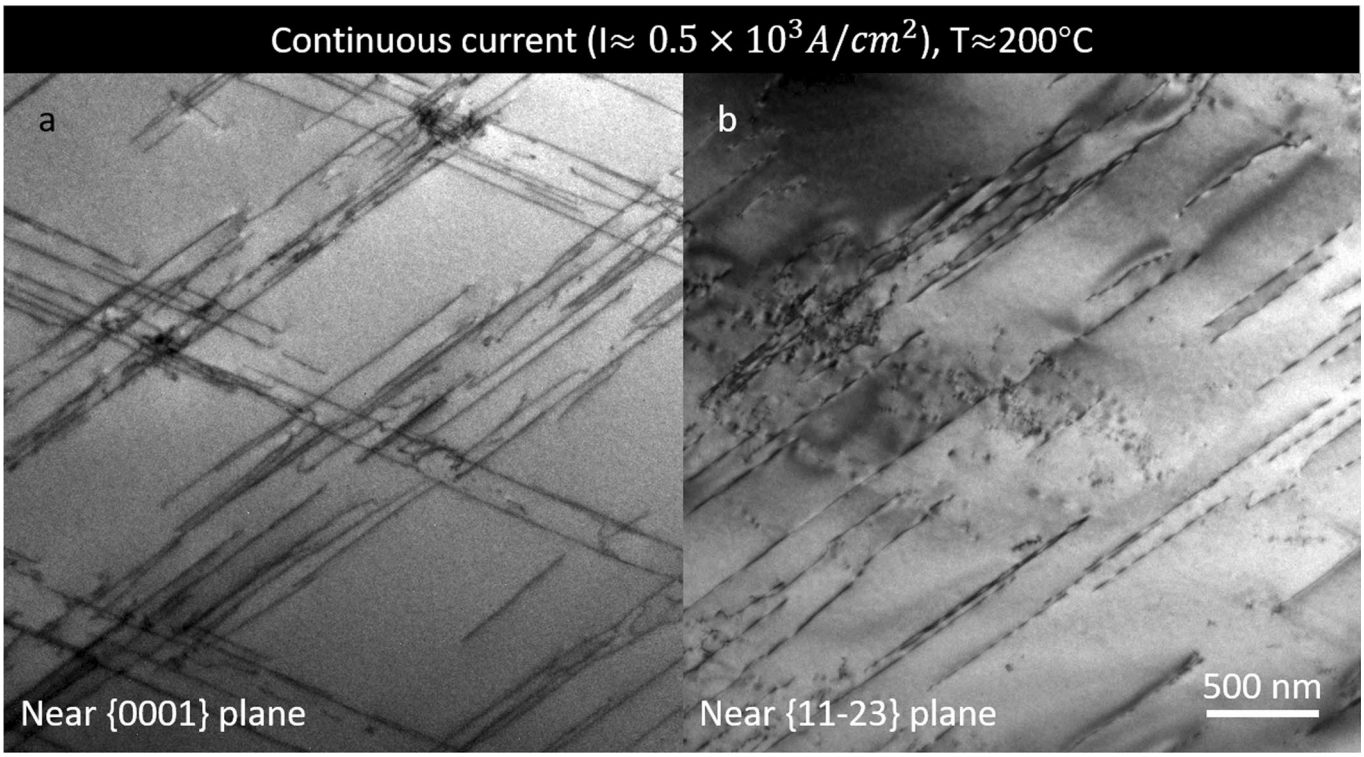

Extended Data Fig. 2 | Planar dislocation configuration of materials subjected to continuous current. a, Imaging condition near the basal plane and (**b**), imaging condition near the {11–23} plane. *This Figure illustrates the dislocation structure deformed under continuous current (current density similar to the pulsing deformation reported in the main text). The temperature during deformation is measured to be around 200 °C. It is shown clearly, in two distinctive imaging conditions (A-near the basal plane, and B-near the {11–23} plane), that the dislocation exhibits a planar configuration, indicating a lack of cross-slip and is very similar to the deformation at room temperature. This suggests that raising temperature at this range cannot trigger planar-to-wavy transition.*

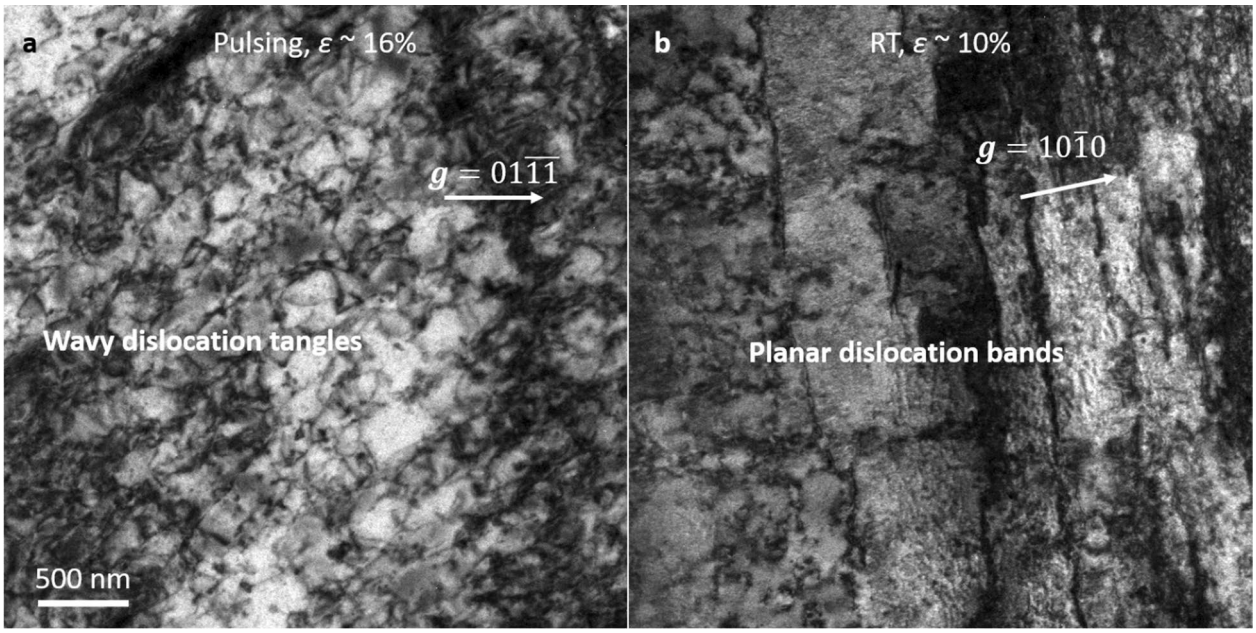

Extended Data Fig. 3 | Dislocation configuration from the as fractured tensile specimen. a, high density of wavy dislocation tangles in pulsing deformed sample; (**b**) Planar dislocation bands in sample deformed at room temperature (RT).

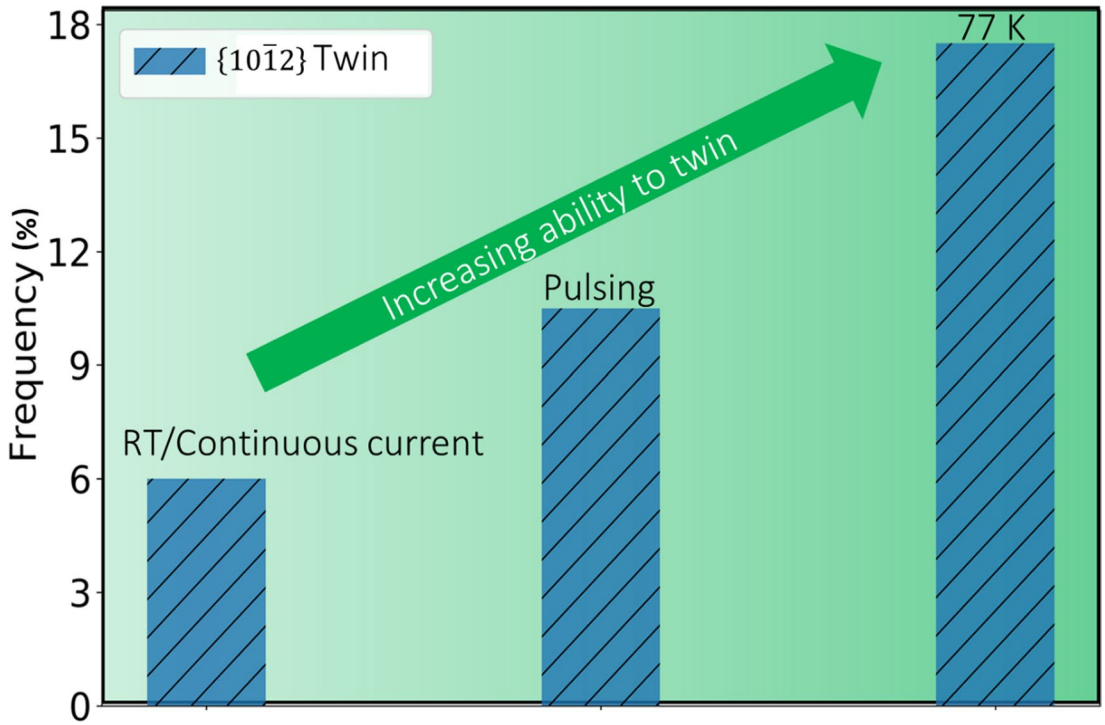

Extended Data Fig. 4 | Comparison of twinning ability in the different deformation conditions. EBSD grain boundary misorientation analysis shows that both electrical pulsing and cryogenic deformation temperature lead to an enhanced twinning ability for the Ti-7Al alloy. The field of view of the EBSD scans is 200 μm × 500 μm along the gauge section of the tensile samples.

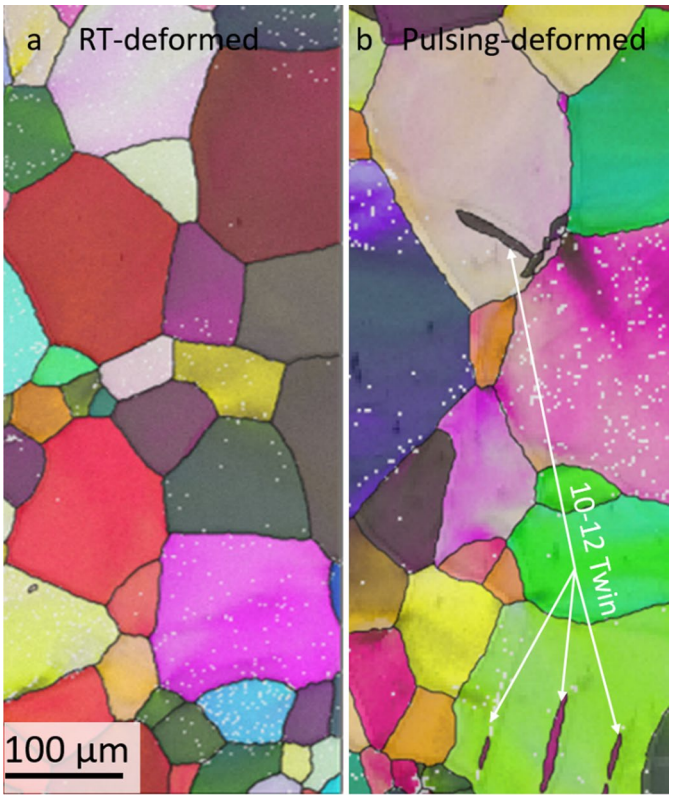

Extended Data Figure 5 | Inverse pole figure mapping of pulsing vs. no-pulsing deformed sample. It shows virtually no twins in the RT-deformed sample (**a**), whereas noticeable {10–12} twins are observed in the pulsing-deformed sample.

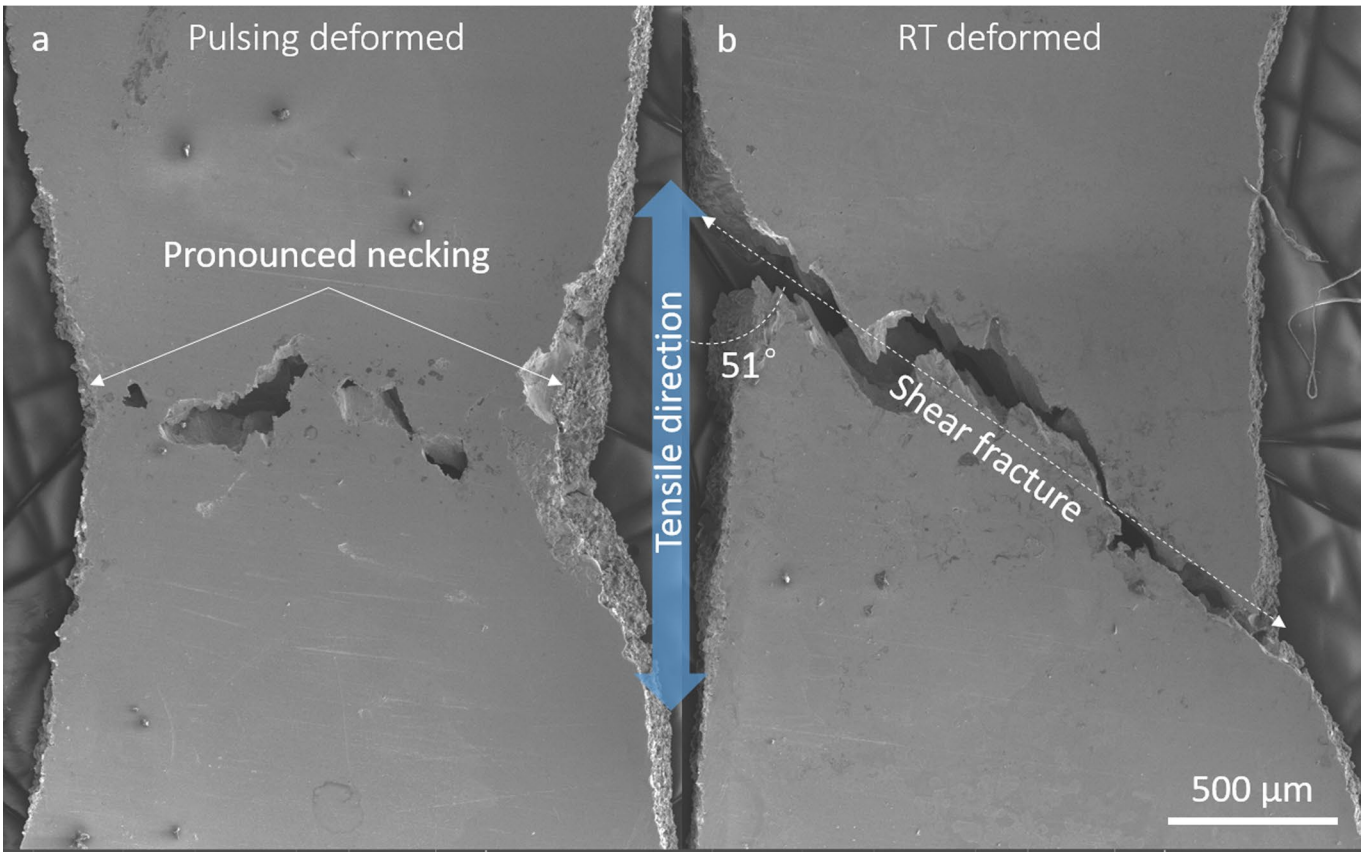

Extended Data Fig. 6 | Secondary electron fractographic micrographs. a, tensile sample after pulsing deformation and (**b**) tensile sample without pulsing treatment.

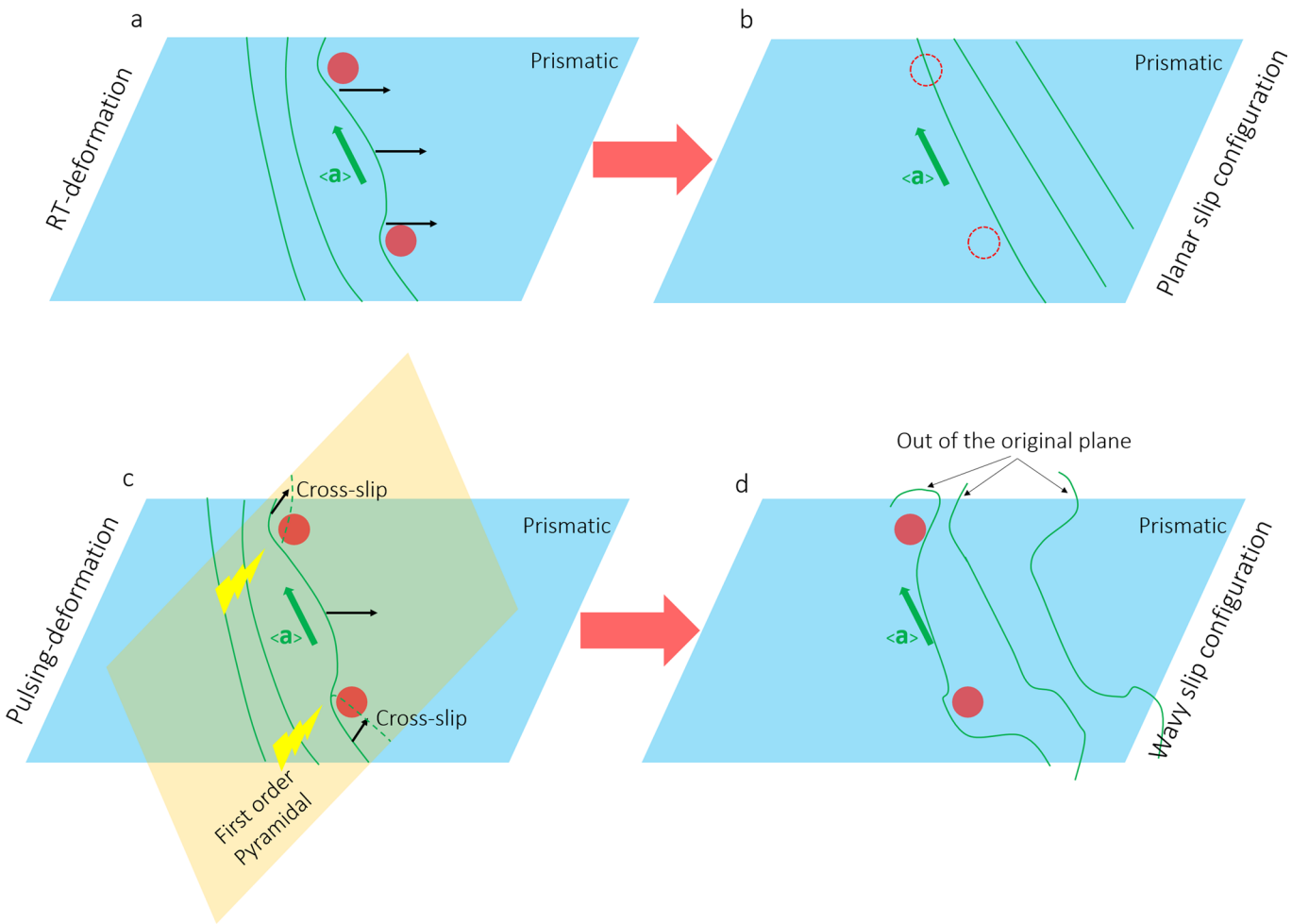

Extended Data Fig. 7 | Schematic illustration of dislocation configurations. a, At room temperature, dislocation prefer to slip on the prismatic plane and cut through the obstacles (Red, solute atoms or short-range order clusters). **b**, The subsequent dislocations tend to follow the leading dislocation due to slip-plane softening, leading to a planar dislocation configuration similar to what is shown in Fig. 2 (**a**, **b**). Note that the obstacles will be destroyed after the passage of several dislocations as each dislocation causes a shear displacement. **c**, Upon applying a pulsed current, dislocation prefer to cross-slip (shown here on the first order pyramidal plane). **d**, This mechanism helps dislocations bypass the obstacles, leading to a non-planar dislocation configuration, similar to what is shown in Fig. 2 (**c**, **d**).

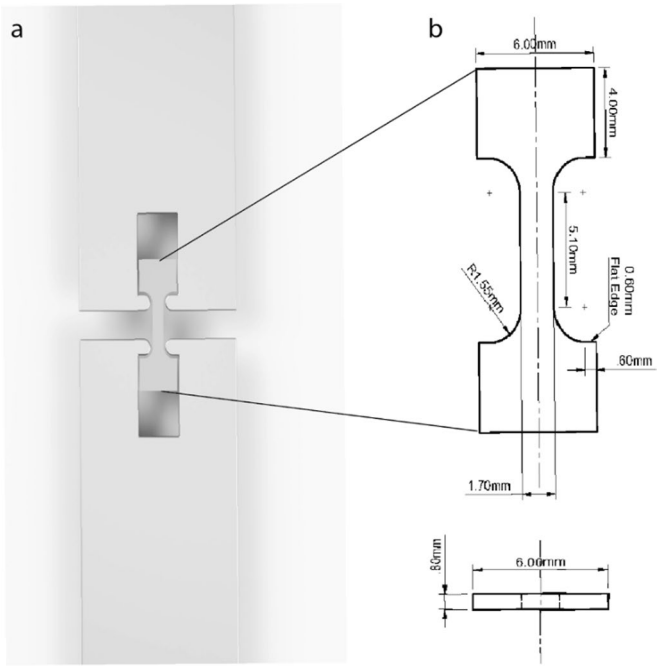

Extended Data Fig. 8 | Detailed illustration of the dog-bone tensile specimen. a, Schematic drawings of the geometry of the sample mounted in our loading fixture; (**b**) the CAD model detailed dimension of the dog-bone sample.